

Supporting Information

Porous Hydrogen Substituted Graphyne for High Capacity and Ultra-Stable Sodium Ion Storage

Ze Yang^a, Chunfang Zhang^b, Zhufeng Hou^c, Xin Wang^a, Jianjiang He^a, Xiaodong Li^a,
Yuwei Song^d, Ning Wang^a, Kun Wang^a, Huanlei Wang^d, and Changshui Huang^{a,*}

^aQingdao Institute of Bioenergy and Bioprocess Technology, Chinese Academy of
Sciences, No. 189 Songling Road, Qingdao 266101, PR China

^bHebei University, Baoding 071002, P. R. China.

^cNational Institute for Materials Science (NIMS), 1-2-1 Sengen, Tsukuba, Ibaraki
305-0047, Japan.

^dOcean University of China, Qingdao 266101, P. R. China.

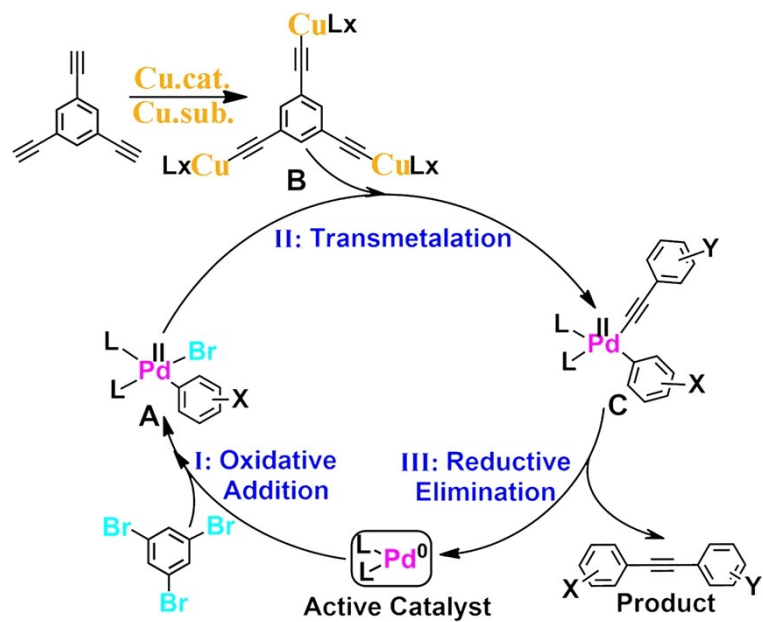


Fig. S1. Proposed reaction mechanism for the cross-coupling reaction of synthesizing HsGY.

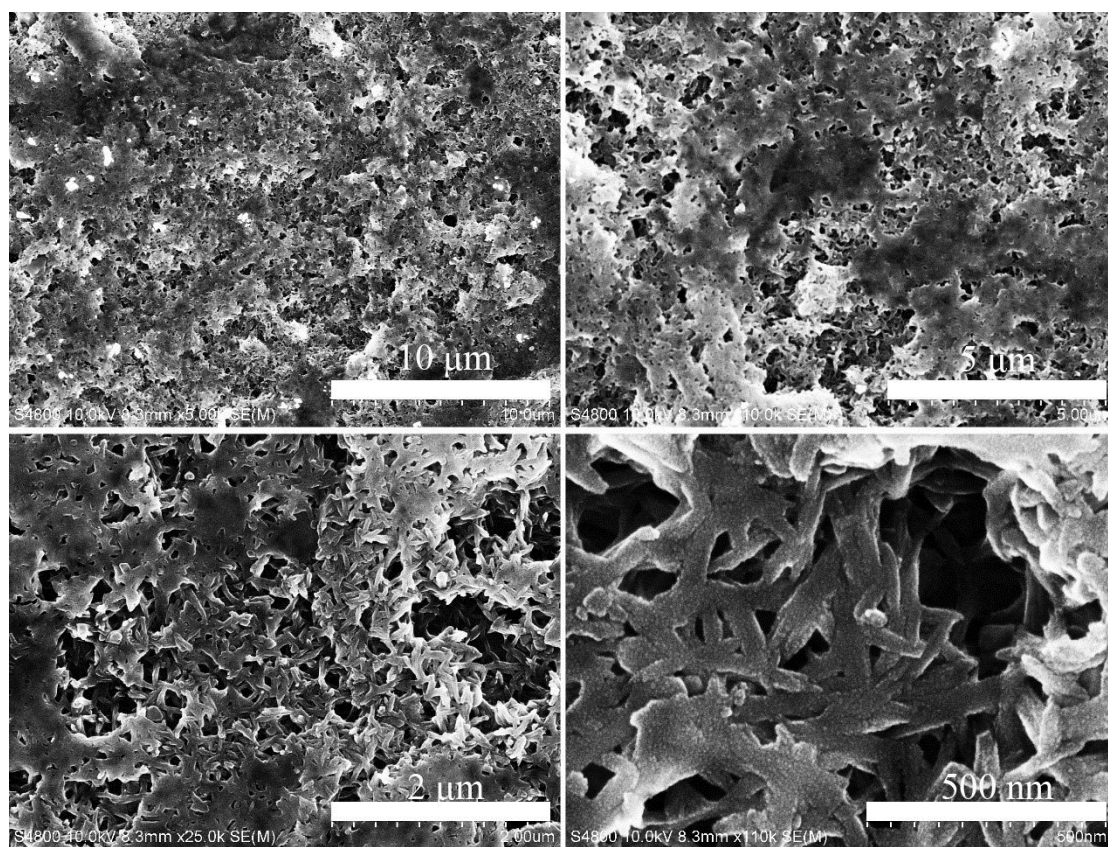


Fig. S2. SEM images with different resolutions of HsGY films. Scale bar: 10 μm (a), 5 μm (b), 2 μm (c), 0.5 μm (d).

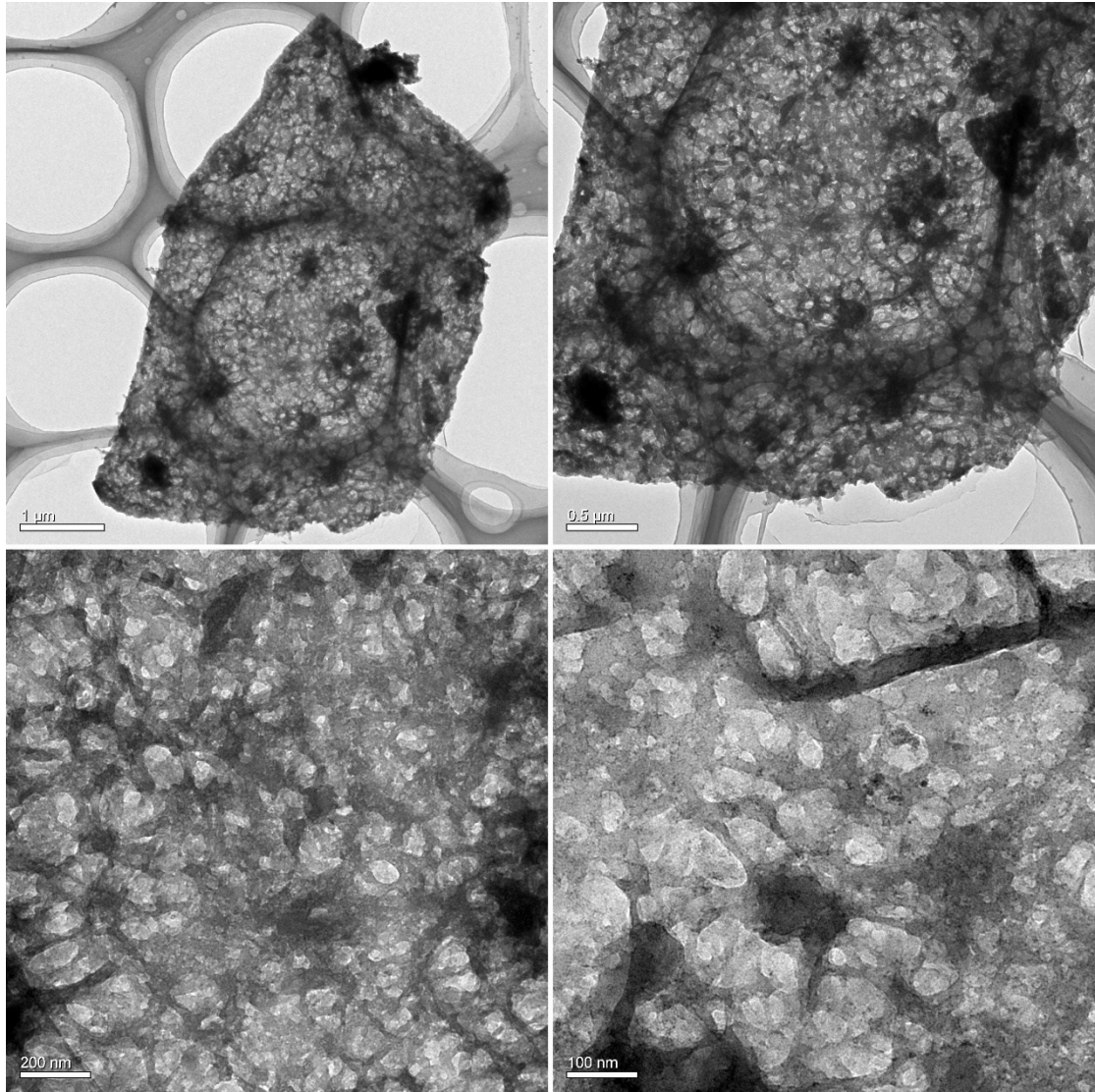


Fig. S3. TEM images with different resolutions of HsGY films.

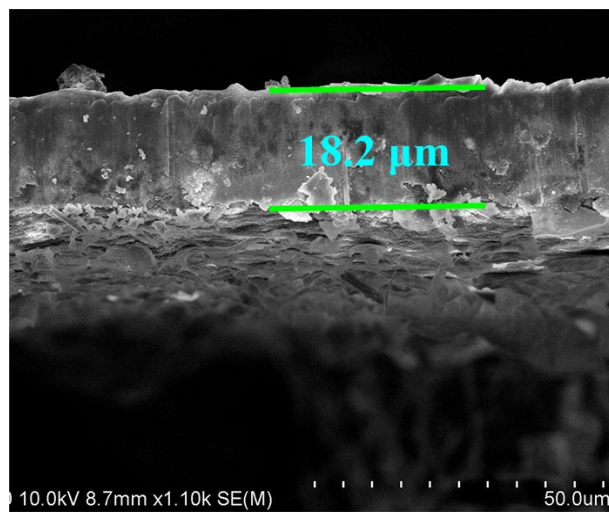


Fig. S4. Cross-section SEM image of the as-prepared HsGY film with the thickness of 18.2 μm.

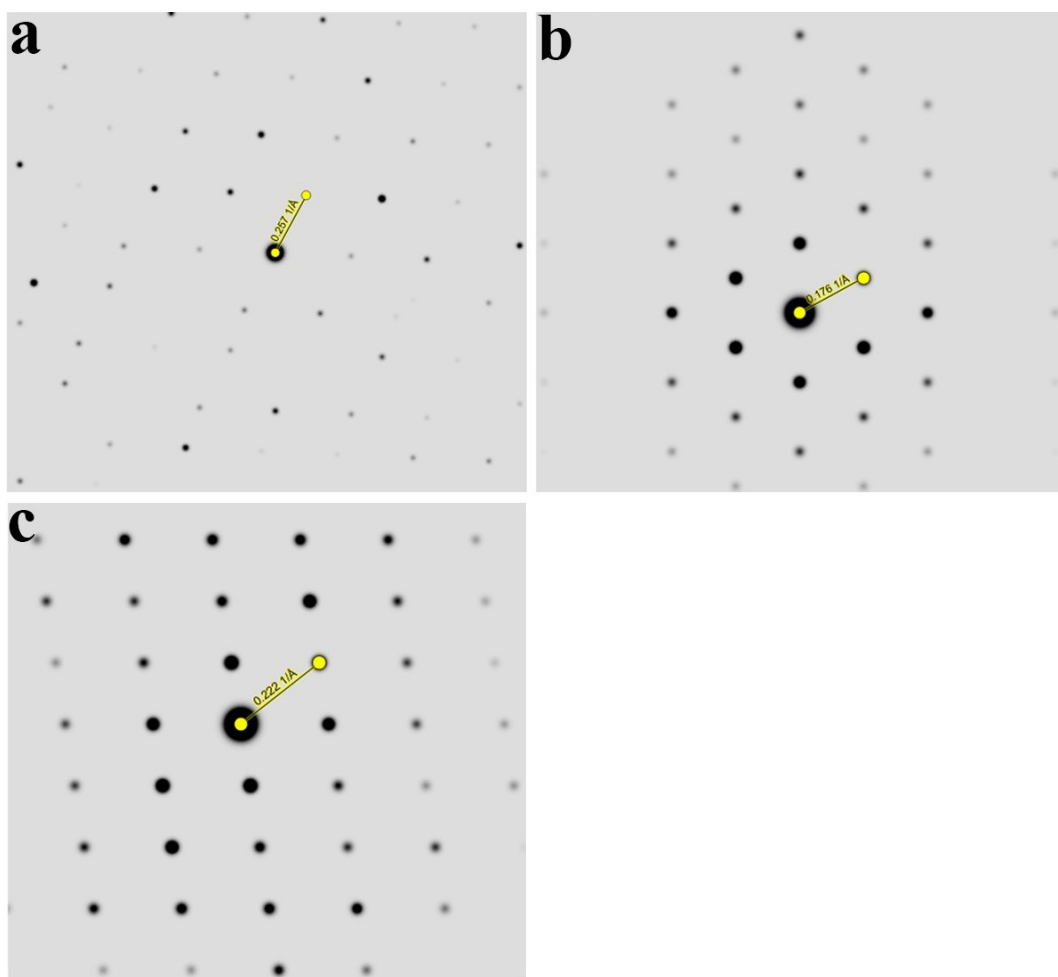


Fig. S5. Three simulated SAED patterns of stacked models for HsGY. Simulated SAED patterns of AB ($a/3, 0$) (a), AB ($2a/3, b/3$) (b) and ABC ($a/3, b/3$) (c) stacked models for HsGY, where a and b are the lattice translation vectors in the x and y directions.

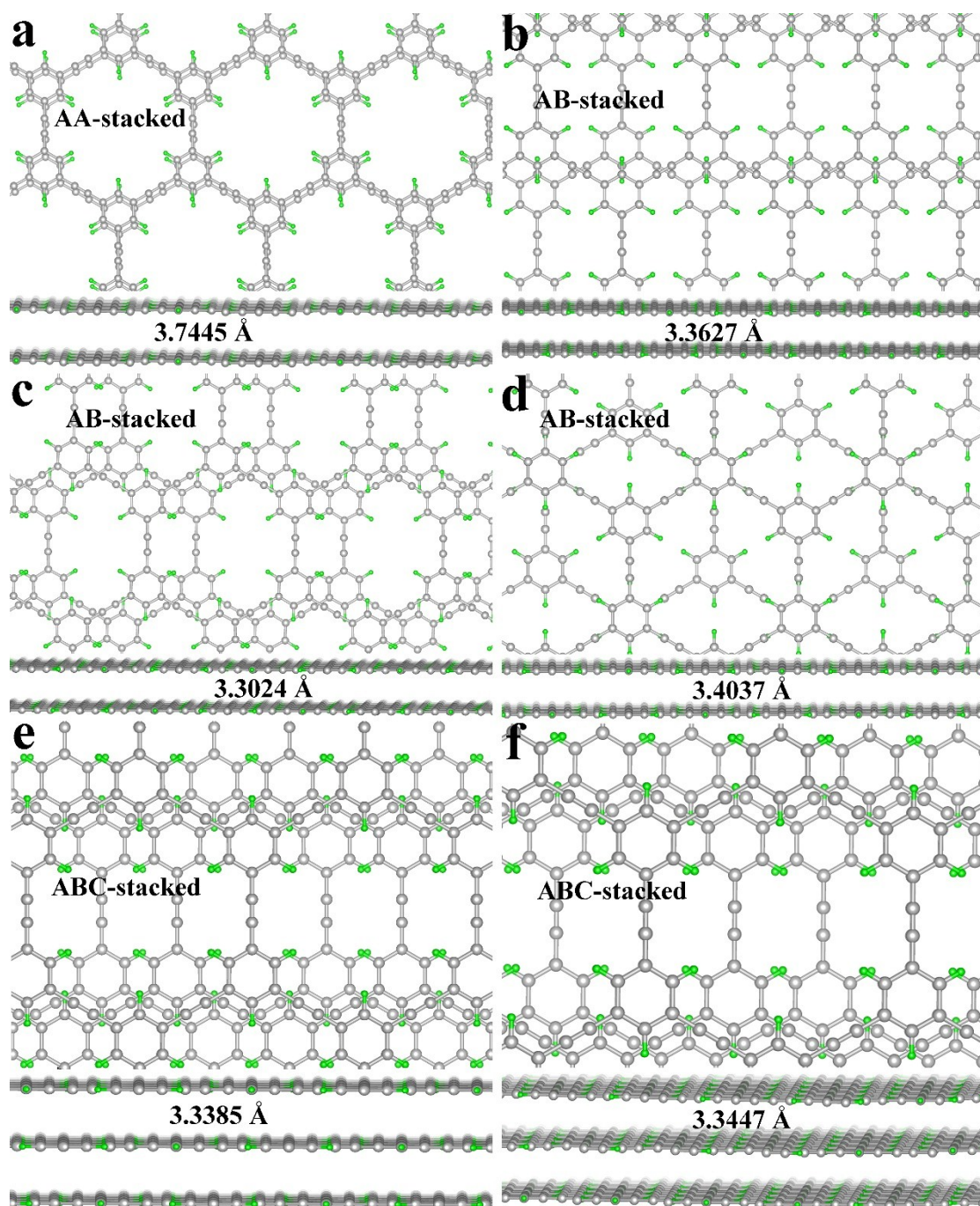


Fig. S6. Six stacked configurations with the corresponding layer-to-layer distance. (a) The AA-type structure of bulk HsGY; (b-d) The AB-type structure of bulk HsGY, the “B” layer is shifted with respect to the “A” layer by $(a/3, 0)$, $(a/2, b/2)$, and $(2a/3, b/3)$; (e-f) The ABC-type structure of bulk HsGY, the “C” (“B”) layer is shifted with respect to the “B” (“A”) layer by $(a/3, 0)$, $(a/3, b/3)$, where a and b are the lattice translation vectors.

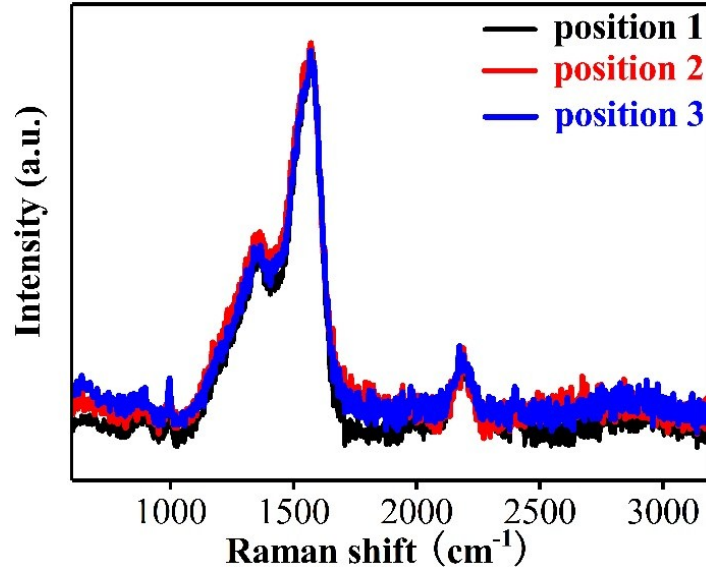


Fig. S7. Raman spectra of HsGY obtained at different positions.

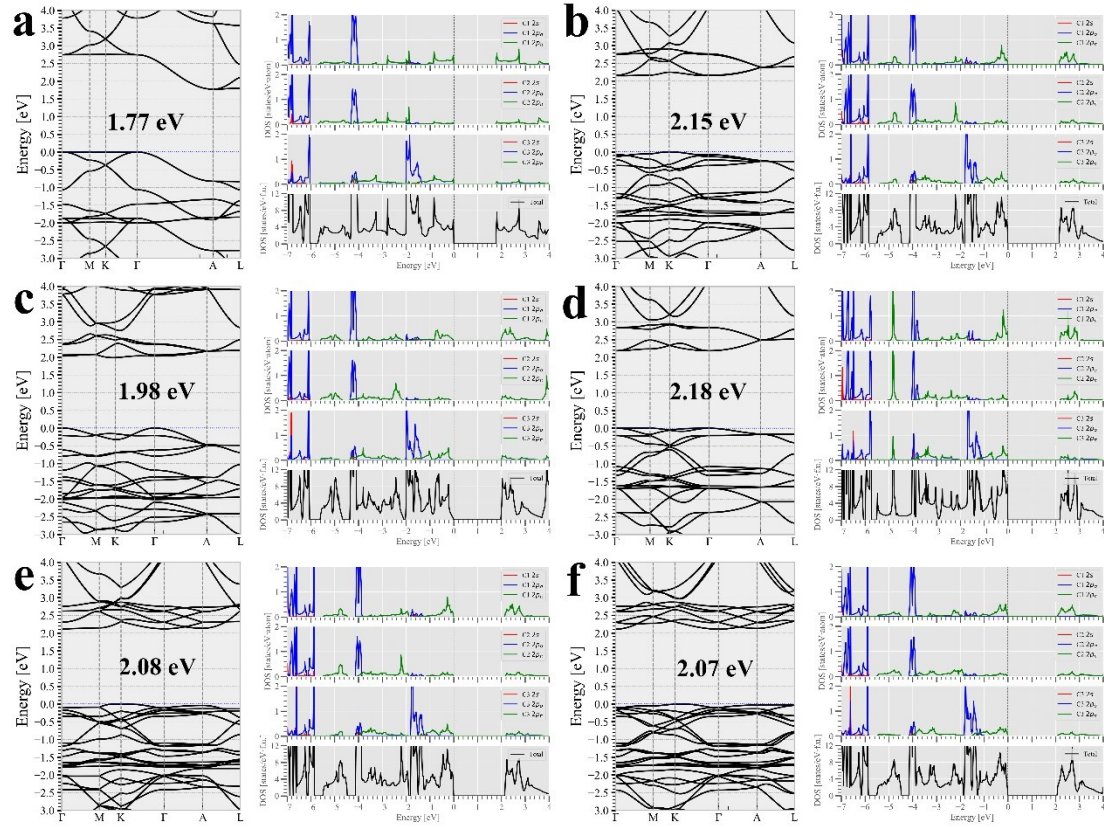


Fig. S8. Calculated electronic band structure and density of states of the bulk HsGY. (a) AA-type; (b) AB-type with the “B” layer shifted with respect to the “A” layer by $(a/3, 0)$; (c) AB-type with the “B” layer shifted with respect to the “A” layer by $(a/2, b/2)$; (d) AB-type with the “B” layer shifted with respect to the “A” layer by $(2a/3, b/3)$; (e) ABC-type with the “C” (“B”) layer is shifted with respect to the “B” (“A”) layer by $(a/3, 0)$; (f) ABC-type with the “C” (“B”) layer is shifted with respect to the “B” (“A”) layer by $(a/3, b/3)$. Calculated values of the band gap were listed in each stacked type.

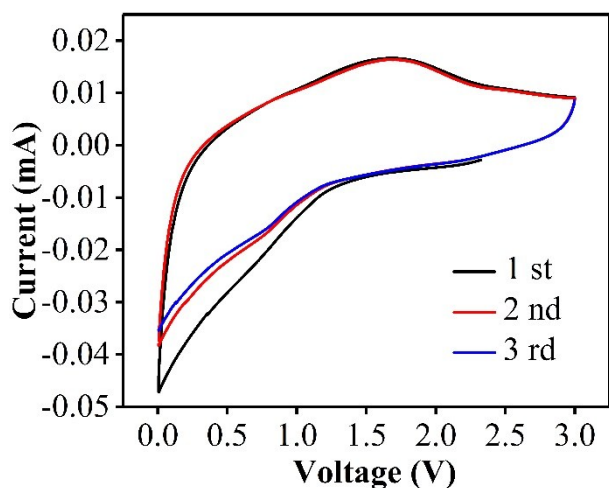


Fig. S9 Cyclic voltammetry curves of a HsGY based electrode, recorded at a scan rate of 0.2 mV s^{-1} between 0.005 and 3 V using a LAND battery testing system. During the first cathodic scan, an irreversible CV band around 0-1.0 V, which can be attributed to the formation process of SEI film and the insertion or desertion reaction of sodium ions into or from the HsGY layers. This phenomenon is perfectly consistent with the charge-discharge profiles (Fig. 4c). The inconspicuous peaks in the CV of the sample imply that the capacity is mainly dominated by faradaic pseudocapacitance because of the high specific surface area.¹

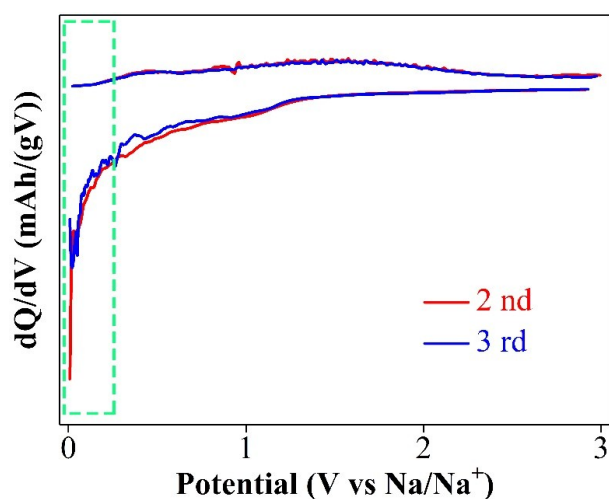


Fig. S10 Differential curves of charge/discharge profiles of the HsGY based electrode at a current density of 100 mA g^{-1} of the 2nd and 3rd cycles. The specific capacity in

the region below 0.2 V can be attributed to the Na⁺ intercalation into HsGY layers, and the capacity above 0.2 V is related to Na ion adsorption on surface active sites as “adsorption-insertion” mechanism.²⁻⁴

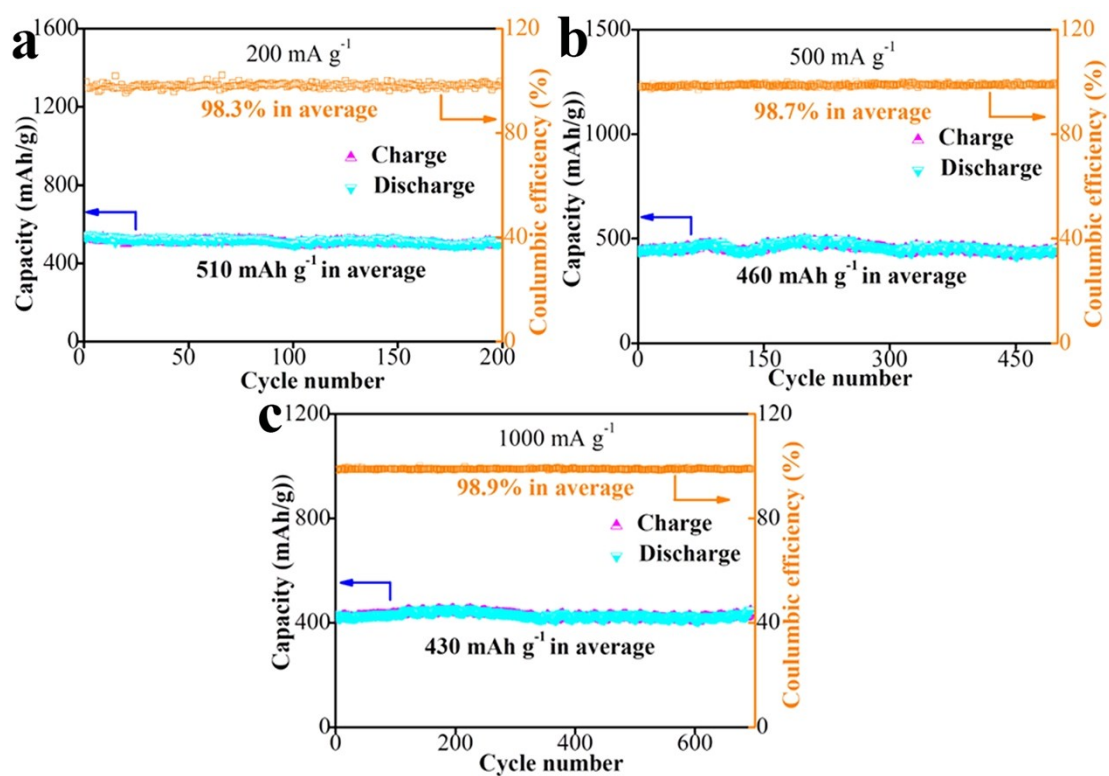


Fig. S11. Cycle performance of HsGY-based electrodes for SIBs under 200 (b), 500 (d) and 1000 (f) mA g⁻¹.

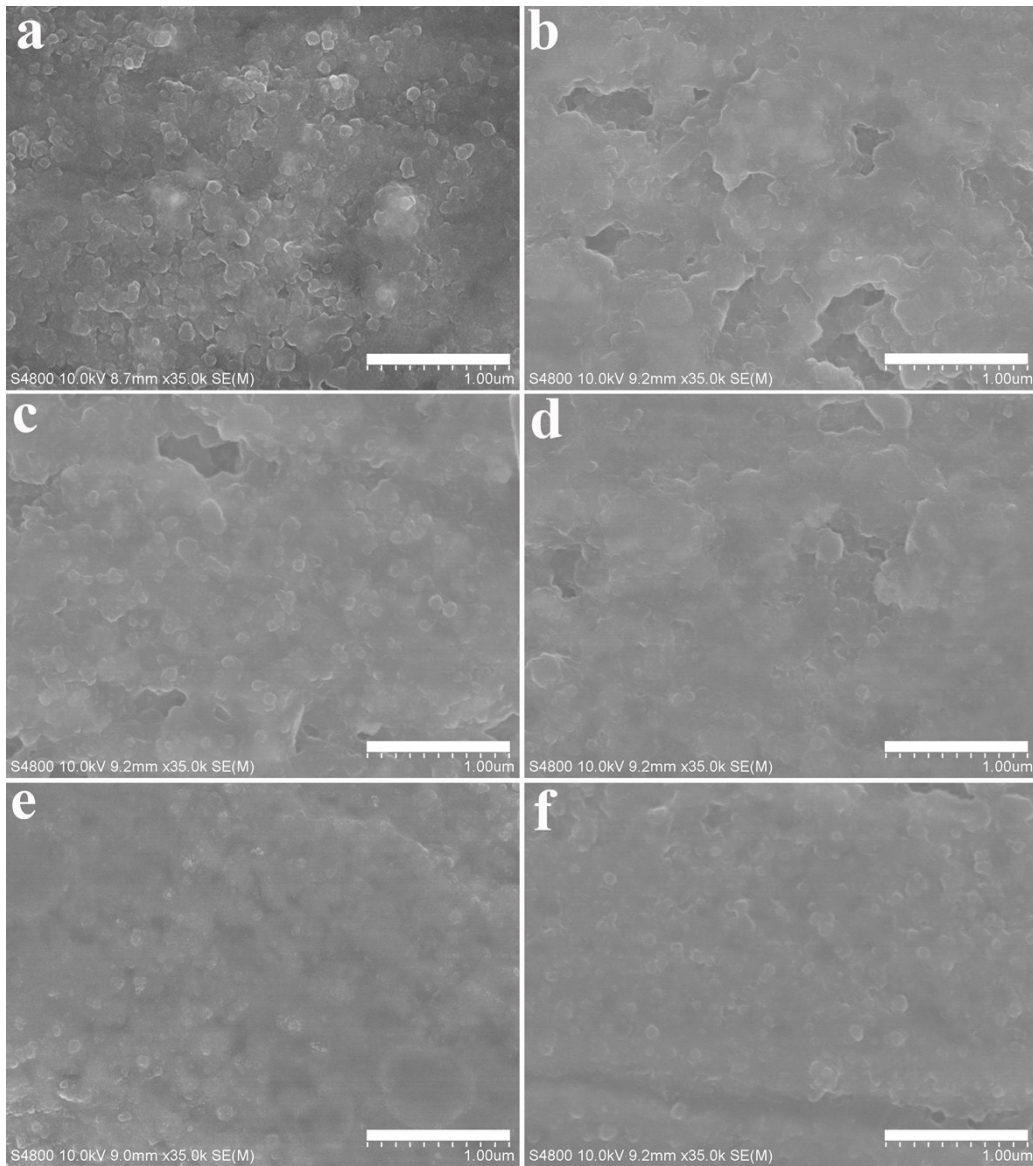


Fig. S12. SEM images of HsGY-based electrodes after 5 (a), 10 (b), 20 (c), 50 (d), 100 (e) and 500 (f) charge/discharge cycles under 500 mA g^{-1} .

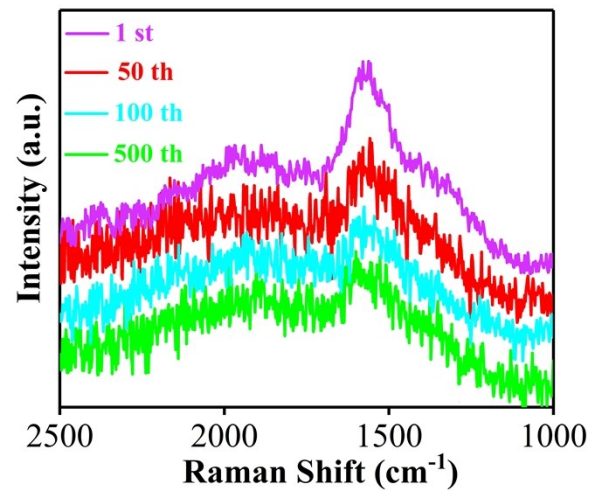


Fig. S13. Raman spectra of HsGY-based electrodes after 1, 50, 100 and 500 charge/discharge cycles under 500 mA g^{-1} .

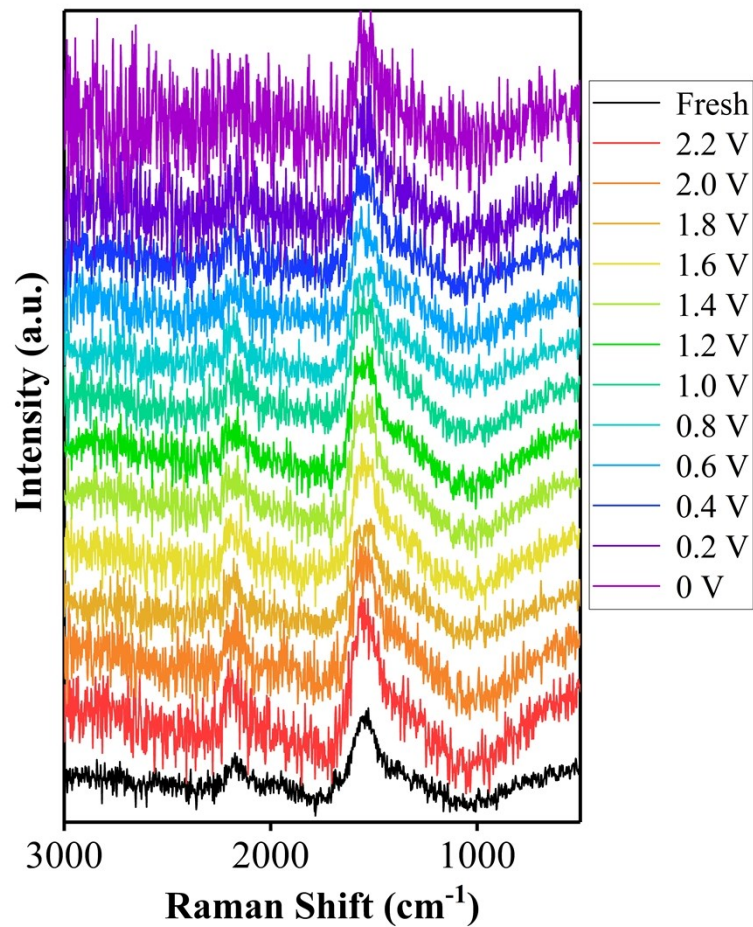


Fig. S14. Raman spectra of HsGY-based electrodes after 1, 50, 100 and 500 charge/discharge cycles under 500 mA g^{-1} .

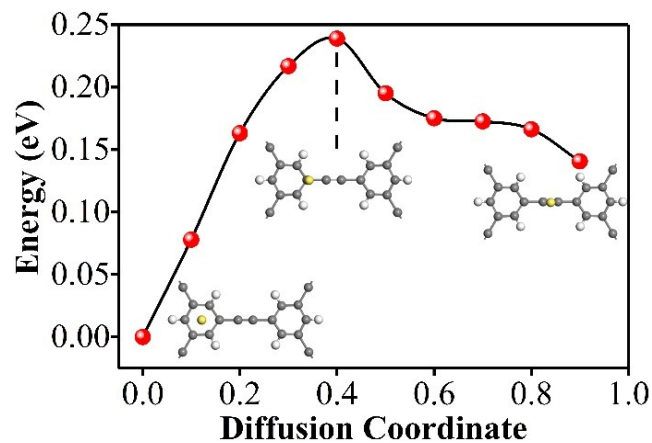


Fig. S15. The energy barrier ΔE of Na atom diffusion. Insets show the local geometry of adsorbed Na atom in the initial state, saddle point and intermediate point of diffusion path. The energy barrier ΔE of Na diffusion was calculated via ab initio calculation. The climbing image nudged elastic band (CI-NEB) method^{5, 6} was used to seek the

saddle points and minimum energy path. Eight images were inserted between beginning and last geometry. Each image is relaxed until the force on each atom is less than 0.02 eV/Å.

Table S1. Comprehensive overview of carbon-based anode materials in SIBs.

Electrode	Reversible capacity (mA h g ⁻¹)	Discharge rate (mA g ⁻¹ or C)	Ref.
HsGY	600	100	This work
HsGY	510	200	This work
HsGY	460	500	This work
HsGY	430	1000	This work
HsGDY	360	1000	ref. ¹
N-CHTs	346	120	ref. ⁷
NG	150	100	ref. ⁸
PCG	400	50	ref. ⁹
N-GF	594	500	ref. ¹⁰
GDY	261	50	ref. ¹¹
CNF	244	100	ref. ¹²
N-CNF	377	100	ref. ¹³
HC	326	0.1C	ref. ¹⁴
Zn-PTCA	357	50	ref. ¹⁵

HsGDY, hydrogen substituted graphdiyne; N-CHTs, N-carbon hollow tubules; NG, natural graphite; PCG, porous carbon/graphene; N-GF, N-doped graphene foams; CNF, carbon nanofiber; N-CNF, N-doped carbon nanofiber; HC, hard carbon; Zn-PTCA, zinc perylenetetracarboxylates.

References

1. J. He, N. Wang, Z. Cui, H. Du, L. Fu, C. Huang, Z. Yang, X. Shen, Y. Yi, Z. Tu and Y. Li, *Nat. Commun.*, 2017, **8**, 1172.
2. S. Qiu, L. Xiao, M. L. Sushko, K. S. Han, Y. Shao, M. Yan, X. Liang, L. Mai, J. Feng, Y. Cao, X. Ai, H. Yang and J. Liu, *Adv. Energy Mater.*, 2017, **7**, 1700403.
3. D. Saurel, B. Orayech, B. Xiao, D. Carriazo, X. Li and T. Rojo, *Adv. Energy Mater.*, 2018, **8**, 1703268.
4. L. Xiao, H. Lu, Y. Fang, M. L. Sushko, Y. Cao, X. Ai, H. Yang and J. Liu, *Adv. Energy Mater.*, 2018, **8**, 1703238.
5. G. Henkelman, B. P. Uberuaga and H. Jónsson, *J. Chem. Phys.*, 2000, **113**, 9901-9904.
6. G. Henkelman and H. Jónsson, *J. Chem. Phys.*, 2000, **113**, 9978-9985.
7. Y. Chen, X. Li, K. Park, W. Lu, C. Wang, W. Xue, F. Yang, J. Zhou, L. Suo, T. Lin, H. Huang, J. Li and J. B. Goodenough, *Chem*, 2017, **3**, 152-163.
8. H. Kim, J. Hong, Y.-U. Park, J. Kim, I. Hwang and K. Kang, *Adv. Funct. Mater.*, 2015, **25**, 534-541.

9. Y. Yan, Y.-X. Yin, Y.-G. Guo and L.-J. Wan, *Adv. Energy Mater.*, 2014, **4**, 1301584.
10. J. Xu, M. Wang, N. P. Wickramaratne, M. Jaroniec, S. Dou and L. Dai, *Adv. Mater.*, 2015, **27**, 2042-2048.
11. S. L. Zhang, J. J. He, J. Zheng, C. S. Huang, Q. Lv, K. Wang, N. Wang and Z. G. Lan, *J. Mater. Chem. A*, 2017, **5**, 2045-2051.
12. Z. Zhang, J. Zhang, X. Zhao and F. Yang, *Carbon*, 2015, **95**, 552-559.
13. S. Wang, L. Xia, L. Yu, L. Zhang, H. Wang and X. W. D. Lou, *Adv. Energy Mater.*, 2016, **6**, 1502217.
14. A. Ponrouch, A. R. Goñi and M. R. Palacín, *Electrochem. Commun.*, 2013, **27**, 85-88.
15. Y. Liu, X. Zhao, C. Fang, Z. Ye, Y.-B. He, D. Lei, J. Yang, Y. Zhang, Y. Li, Q. Liu, Y. Huang, R. Zeng, L. Kang, J. Liu and Y.-H. Huang, *Chem*, 2018, **4**, 2463-2478.